

Detection of the Spin-Chemical Potential in Topological Insulators Using Spin-Polarized Four-Probe STM

Saban M. Hus,¹ X.-G. Zhang,² Giang D. Nguyen,¹ Wonhee Ko,¹ Arthur P. Baddorf,¹ Yong P. Chen,³ and An-Ping Li^{1,*}

¹Center for Nanophase Materials Sciences, Oak Ridge National Laboratory, Oak Ridge, Tennessee 37831, USA

²Department of Physics and the Quantum Theory Project, University of Florida, Gainesville, Florida 32611, USA

³Department of Physics and Astronomy, Purdue University, West Lafayette, Indiana 47907, USA

(Received 9 January 2017; revised manuscript received 10 August 2017; published 27 September 2017)

We demonstrate a new method for the detection of the spin-chemical potential in topological insulators using spin-polarized four-probe scanning tunneling microscopy on *in situ* cleaved Bi₂Te₂Se surfaces. Two-dimensional (2D) surface and 3D bulk conduction are separated quantitatively via variable probe-spacing measurements, enabling the isolation of the nonvanishing spin-dependent electrochemical potential from the Ohmic contribution. This component is identified as the spin-chemical potential arising from the 2D charge current through the spin momentum locked topological surface states (TSS). This method provides a direct measurement of spin current generation efficiency and opens a new avenue to access the intrinsic spin transport associated with pristine TSS.

DOI: 10.1103/PhysRevLett.119.137202

Topological insulators (TIs) belong to a new class of matter with nontrivial surface states, in which the axis of spin quantization and the momentum of charge carriers are perpendicularly locked to each other [1–3]. Such spin-momentum locking does not only provide a topological protection against backscattering, but also makes the electrical current carried by these topological surface states (TSS) intrinsically spin polarized [4]. Currents with spin polarizations that are momentum locked can be a treasure trove for new fundamental physics [5,6] and offer a distinct possibility for a highly efficient spin current generation [7]. For both the understanding of the spin-momentum locking and the development of TI-based spintronic devices, it is essential to directly detect the spin current and measure the efficiency of spin current generation.

Early experimental confirmations of spin-momentum locking in TSS were obtained by spin-angle resolved photoemission spectroscopy (spin ARPES) [8–10] and spin-polarized photocurrent studies [11], both of which are highly sensitive to surface states. Notwithstanding these early successes, all-electrical detection of spin polarization of TSS is more challenging due to the existence of a conduction channel through the bulk, although such detection is more relevant to practical applications.

In recent years several studies based on the difference of the quasi-Fermi level of electrons with opposite spin directions were able to detect the spin polarization of the currents carried by TSS [12–17]. In all of these electrical detection approaches, the contacts were fabricated with lithographically defined ferromagnetic (FM) metals and the spin sensitive component of conductance was differentiated by controlling the polarization of the FM contacts with an external magnetic field. However, these measurements potentially suffer from several extrinsic effects. First,

surface absorbents even by residual gas molecules in the vacuum environment [18–20] are found to change the carrier density of some TI materials, which may alter the electronic structure of the surface and affect the net spin polarization of the current carried by surface states. Second, in many 3D TIs the bulk channel dominates the electron transport (even though nominally insulating) and makes it difficult to quantitatively measure the conduction through the surface states. Transport measurements performed with fixed contacts are incapable of distinguishing between the surface and bulk conductivities, encumbering quantitative measurement of the spin polarization of the current. Furthermore, several studies with lithographically defined contacts have shown that nominally identical results can also appear even in topologically trivial materials such as gold [21] or arise from fringe-field-induced Hall voltages [22], and their origins are not due to current-induced spin polarization of the carriers in TSS. These issues make alternative transport measurements vital for the electrical detection of charge-current-induced spin polarization in TIs and can be addressed by *in situ* transport measurements with a four-probe scanning tunneling microscope (four-probe STM) [23,24].

Here we report the direct observation of a spin-chemical potential induced by a charge current flowing through TSS. The observation is enabled by advancing two STM-based techniques, spin-polarized STM [25,26] and four-probe STM [24,27], to achieve spin-sensitive multiprobe transport measurements on pristine topological insulator surfaces in the ultrahigh vacuum (UHV) environment. By examining the potential difference between a FM probe and a nonmagnetic (NM) probe as a function of the spatial separation between them, not only can we differentiate surface and bulk contributions to the conductivity, but also

isolate the nonvanishing spin-dependent electrochemical potential from the Ohmic contribution. Moreover, the spin-sensitive probe method with nanometer scale soft contacts minimizes metal induced effects on the surface. The measured spin chemical potentials directly come from the 2D charge current. In this manner, we achieve a direct and quantitative measurement of the intrinsic spin-polarized transport associated with TSS.

The high-quality $\text{Bi}_2\text{Te}_2\text{Se}$ single crystals used in this study were synthesized by the Bridgman technique with n -type doping, similar to those previously reported [28,29]. Samples were cleaved *in situ* in the UHV chamber at room temperature and immediately transferred to the four-probe STM stage for transport measurements. Four probe spectroscopy measurements were performed with STM tips (W or Ni with varying magnetization directions) placed in a collinear configuration on the surface at around $82(\pm 1)$ K [23,29]. To create fresh surfaces, samples were exfoliated (*in situ*) for each set of measurement, with experimental details in the Supplemental Material [30].

The Fermi energy (E_F) of TSS is located within the bulk band gap and above the Dirac point [28]. In the absence of a net current, the electrons at the Fermi level homogeneously occupy the Fermi circle centered at the $(k_x, k_y) = (0, 0)$ point, without net momentum and spin polarization. However, a current (I) carried by TSS creates an imbalance in the electron momentum which can be seen as a shift of Fermi circle as illustrated in Fig. 1(a). Because of the spin-momentum locking, the shift of the Fermi circle also creates a spin accumulation with the spin moment perpendicular to both the current direction and the surface normal. Hence, a FM probe which is sensitive only to electrons with a fixed polarization will measure a different electrical potential than an NM probe placed at the same point. Because the electron spin is not aligned along a single axis, a simple spin-dependent electrochemical potential as defined in Ref. [34] is inadequate. We thus invoke a vector spin-chemical potential [35,36], defined as $\vec{h} = (\mu_\uparrow - \mu_\downarrow)\hat{h}$, where \hat{h} is the direction of the net spin polarization and μ_\uparrow and μ_\downarrow are the energy levels of the two extremal points of the quasi-Fermi surface as indicated in Fig. 1(a). The energy of an electron with spin \vec{s} due to the spin-chemical potential is given by $(\mu_\downarrow + \vec{s} \cdot \vec{h})$ in units of eV [37], where $\mu_\downarrow = (\mu_\uparrow + \mu_\downarrow)/2$ is the Ohmic component of the total chemical potential of the electrons, namely, the charge chemical potential.

Assuming that the electron density does not change during a constant current measurement, $|\vec{h}|$ is related to the difference (ΔV_s) between the potentials measured by a FM and an NM probe placed at the same point, as illustrated in Fig. 1(b), and can be derived as (see Supplemental Material [30])

$$|\vec{h}| = \frac{4|\Delta V_s|}{P_{\text{FM}}} \left(1 + \frac{e\Delta V_s}{2\mu_F} \right) = -p[(\hat{n} \times \hat{I}) \cdot \hat{M}] \frac{8\pi\hbar}{e^2} \frac{1}{k_F} |J_x|, \quad (1)$$

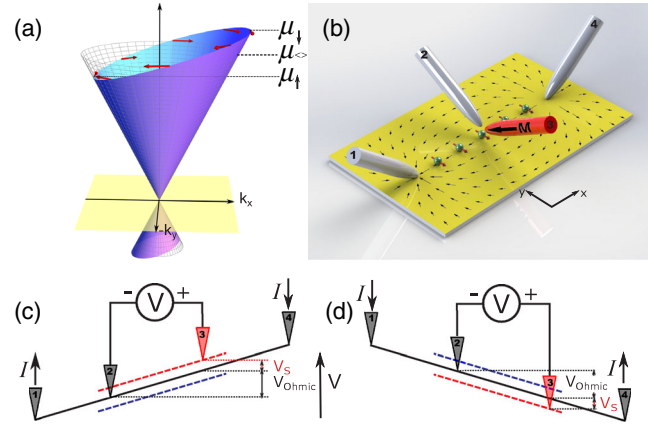


FIG. 1. (a) Illustration of Dirac-like dispersion and helical spin texture of TSS in 3D TIs in an electric field along the $-x$ direction. Spin orientations are shown with red arrows. The equilibrium Fermi surface under zero electric field is shown with a gray meshed surface. (b) Conceptual drawing of spin-polarized four-probe STM transport measurements. The current is supplied by the pointlike source and drain probes (1 and 4) and the local electrochemical potential is measured by the probes in the middle (2 and 3). The electrochemical potential measured by a nonmagnetic probe (gray) averages over all spin directions while the potential measured by a ferromagnetic probe (red) is sensitive to a particular spin direction. (c) Illustration of the electrical potential measured by nonmagnetic probes (black line) and ferromagnetic probes with magnetizations parallel and antiparallel to the current induced spin polarization of the TSS. (d) When the current direction is reversed, both the Ohmic and the spin voltages change sign making $V(-I) = -V(I)$.

where k_F is the Fermi wave vector, and μ_F is the Fermi energy with respect to the Dirac point. J_x is the density of charge current carried by TSS at the measurement position, \hat{n} , \hat{I} , \hat{M} are the unit vectors along the surface normal, current direction, and probe magnetization, respectively, p is the spin polarization value of the current, and P_{FM} is the effective spin sensitivity of the FM probe. The minus sign comes from the convention that the magnetic moment of the STM tip is opposite to the majority spin orientation of the tip [38]; namely, if an FM material is magnetized along $+\hat{y}$, its majority spin is oriented along $-\hat{y}$. For $e\Delta V_s \ll \mu_F$, the second equality reduces to the linear result derived by Hong *et al.* [39]. Figure 1(c) illustrates the electrical potential between the source and the drain (outer) probes in a case where J_x is constant. The electrical potentials for s_\uparrow and s_\downarrow channels are shown with red and blue dashed lines, respectively. The black solid line represents the charge chemical potential measured by a NM probe. Therefore, the potential difference measured between two inner probes (one FM, one NM) consists of two contributions. The first one is created by the Ohmic resistance and vanishes as the distance between the inner probes goes to zero, while the second one originates from the spin polarization of the TI surface states and is independent of the distance between the inner probes. When the current direction

is reversed, both the Ohmic potential between the probes and the relative spin-polarized potentials for s_{\uparrow} and s_{\downarrow} channels are reversed [as illustrated in Fig. 1(d)]. Therefore, the magnitude of the measured potential $\Delta V = V_{\text{Ohmic}} + \Delta V_s$ does not depend on the current direction [i.e., $\Delta V(I) = -\Delta V(-I)$]. On the other hand, when the polarization of the FM probe is reversed, ΔV_s changes the sign but V_{Ohmic} remains unchanged. Hence, by examining the potential difference between the inner probes at a variety of probe positions on the surface of a 3D TI we can extract spin-chemical potential and the net spin polarization of the current carried by the surface states.

We first quantitatively differentiate the 2D conductance of the surface states from the 3D conductance of the bulk counterpart. Earlier attempts of such a problem assumed two decoupled conduction channels corresponding to 2D and 3D [40]. A more realistic model requires the consideration of the coupling between these two channels and should allow a cross channel current at every point along the interface. Such a quantitative differentiation has only recently been available with the development of the four-probe spectroscopy technique [29,41]. In these measurements, four STM tips are used as probes aligned in a collinear configuration. A set of resistance values are acquired when the outer probes are kept in fixed positions and the inner probe distance is varied. With the consideration of the coupling of the surface and the bulk conduction channels, the relationship between the four-probe resistance and the interprobe spacing is given by [29]

$$R = \frac{V_3 - V_2}{I} = \frac{1}{2\pi} \rho_{2D} \ln \left[\frac{(g + \frac{s_{14}}{s_{12}})(g + \frac{s_{14}}{s_{34}})}{(g + \frac{s_{14}}{s_{13}})(g + \frac{s_{14}}{s_{24}})} \right] = \rho_{2D} X_g, \quad (2)$$

where V_i is the measured electrochemical potential of probe i , I is the total current between the source and the drain probes (probes 1 and 4), ρ_{2D} is the surface resistivity, s_{ij} is the distance between the probes i and j , and $g = (\rho_{2D}/\rho_{3D})s_{14}$ is a dimensionless parameter which gives the ratio between the contributions from the 2D surface and the 3D bulk to the total resistance. The relationship between R and X_g is linear only when a correct fitting value of g is found.

Four-probe resistance measured on a fresh (within 24 h of cleavage) surface of $\text{Bi}_2\text{Te}_2\text{Se}$ is presented in Figs. 2(a) and 2(b) for outer probe spacing $s_{14} = 10.9 \mu\text{m}$ and using NM probes and $s_{14} = 6.0 \mu\text{m}$ with an FM probe, respectively. The data can be best fitted with Eq. (2) using $g = 0$, meaning that 100% of the current flows via the 2D surface channel for the given distance between the outer probes. From the slope of these plots we extract ρ_{2D} values of 590 and 627 Ω , respectively. We note that there may still be a very small contribution from the bulk states to the electronic transport. However, such a contribution is outside of our detection window ($g < 0.1$) [29], meaning that for $s_{14} \leq 10.9 \mu\text{m}$ the bulk contribution cannot exceed an upper limit of 10%. At 82 K the bulk conduction becomes

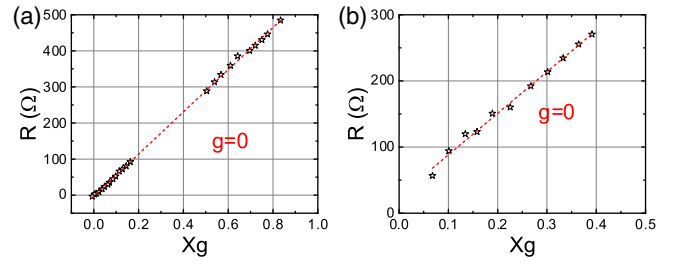


FIG. 2. Measured resistance values R with varying probe spacing plotted as a function of X_g on the surface of $\text{Bi}_2\text{Te}_2\text{Se}$. The source probe spacings are 10.9 and 6.0 μm for (a) and (b), respectively. Both voltage probes are NM in (a) but one is FM in (b). A linear fit between R and X_g can only be obtained when $g = 0$, implying surface dominant transport.

detectable only for $s_{14} \geq 40 \mu\text{m}$ with a measured bulk resistivity value of 2.61 Ωcm , much higher than 0.015 or $\sim 0.1 \Omega \text{cm}$ reported before [29,40].

In the absence of spin sensitivity, the four-probe transport measurements return only the Ohmic resistance. Hence, when the charge transport is in the diffusive limit, if the distance between the inner probes goes to zero the measured resistance also goes to zero. This behavior is trivial and independent of the dimensionality of the system or relative contributions of different conduction channels. Four-probe spectroscopy measurements performed with tungsten probes clearly show such a behavior. For instance, in Fig. 3(a) which presents the details of the Fig. 2(a) for the limit $X_g \rightarrow 0$, a linear fit of R vs X_g data intersects the $X_g = 0$ axis at $R = 0.4 \pm 0.7 \Omega$, namely, R is zero within the experimental accuracy.

We then replaced one of the tungsten (voltage) probes with a FM nickel probe magnetized along its axis by using a permanent magnet before transport measurements [26,42]. As explained above, the potential difference between an NM and a FM probe manifests as a potential offset and a finite resistance as $X_g \rightarrow 0$.

For a collinear probe configuration and a homogenous 2D surface, the current density at the location of a voltage probe 3 can be written as

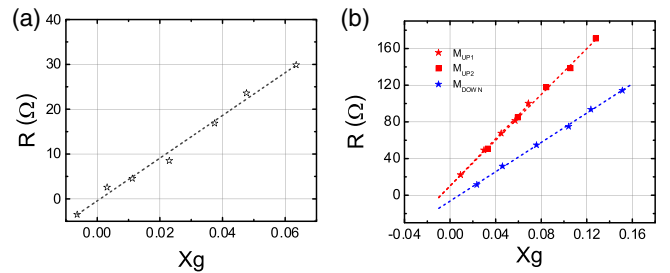


FIG. 3. (a) Spin-averaged four-probe STM transport measurements on the surface of $\text{Bi}_2\text{Te}_2\text{Se}$ with a NM probe. (b) Spin-polarized four-probe STM transport measurements with a FM probe magnetized up on two different surface areas (red squares and stars), and with a FM probe magnetized down on another surface area, respectively.

$$J_x = \frac{1}{2\pi} \left(\frac{1}{s_{13}} + \frac{1}{s_{34}} \right) I, \quad (3)$$

where I is the total current between the source and the drain (probes 1 and 4). If probe 3 is an FM probe, substituting Eq. (3) into Eq. (1), we have,

$$\Delta V_s = Ip[-(\hat{\mathbf{n}} \times \hat{\mathbf{I}}) \cdot \hat{\mathbf{M}}] P_{\text{FM}} \frac{h}{e^2} \frac{1}{2\pi k_F} \left(\frac{1}{s_{13}} + \frac{1}{s_{34}} \right), \quad (4)$$

Because of this potential offset, the measured resistance between an NM and a FM tip placed at the same point should be,

$$\begin{aligned} \lim_{X_g \rightarrow 0} R &= R_s = \frac{\Delta V_s}{I} \\ &= p(-(\hat{\mathbf{n}} \times \hat{\mathbf{I}}) \cdot \hat{\mathbf{M}}) P_{\text{FM}} \frac{h}{e^2} \frac{1}{2\pi k_F} \left(\frac{1}{s_{13}} + \frac{1}{s_{34}} \right). \end{aligned} \quad (5)$$

On a freshly cleaved sample, X_g vs R plots obtained with a nickel probe intersects the $X_g = 0$ axis at finite R_s value of $10.2(\pm 2.8) \Omega$ and $10.1(\pm 3.0) \Omega$ for two different surface areas as shown in Fig. 3(b), indicating the existence of voltage offsets arising from spin chemical potentials.

Linear behavior of the $V(I)$ curves [see Figs. 4(c), 4(d)] shows that measured R values (therefore, R_s) are independent of the current, I . This is expected since the spin density scales linearly with current density when $e\Delta V_s \ll \mu_F$. In our experiments we obtained $\Delta V_s = R_s I \approx 1$ meV for a

source-drain current of $100 \mu\text{A}$. To find μ_F we performed STM measurements on freshly cleaved $\text{Bi}_2\text{Te}_2\text{Se}$ crystals. Topographic STM images [Fig. 4(a)] reveal the hexagonal structure of the surface lattice where vacancies and other (sub) surface defects are also clearly visible. The electronic density of states revealed by scanning tunneling spectroscopy (STS) measurements on this surface show a minimum at -28 meV corresponding to the Dirac point energy with respect to the Fermi level.

Since the current between source and drain probes is carried out only through the 2D surface channel in this measurement, the ratio of spin-polarized current carried by the surface states can be derived directly by using Eq. (4). As the spin polarization of the surface carriers is locked perpendicularly to the current direction, maximized spin sensitivity is achieved when the in-plane component of the tip magnetization is perpendicular to the current direction. Because of the 45° angle between the surface normal and the STM probes, $-(\hat{\mathbf{n}} \times \hat{\mathbf{I}}) \cdot \hat{\mathbf{M}} = \sin(45^\circ)$. Using $P_{\text{FM}} = 0.5$ [43], $v_F = 6.0 \times 10^5$ m/s [28,29], and $\mu_F = 28$ meV, we obtain a k_F value of 7×10^7 m $^{-1}$, which gives $p = 0.81$ and 0.84 from the data with an FM probe magnetized up in Fig. 3(b). By using a Ni probe with reversed magnetization, we obtain an R_s value of $-6.4(\pm 2.8) \Omega$ [Fig. 3(b), blue line]. Indeed, the sign of R_s is reversed too. Using the same parameters as above we get a spin polarization value of $p = 0.50$. The difference in the measured p values may be attributed to the variation of P_{FM} between different probes. While the quantum well states arising from band bending at the TI surface are also spin polarized due to Rashba spin-orbit coupling, the resulting net spin polarization from these trivial states is negligible due to the self-canceling between the pair of Fermi surfaces [39].

One should note that the measured p values merely correspond to the ratio of spin-polarized current over the total surface current. This is different from the net current induced spin polarization of TSS (i.e., $(n_\uparrow - n_\downarrow)/(n_\uparrow + n_\downarrow)$) which has a value in the order of $\Delta V_s/\mu_F$. Moreover, since the measurements are performed in an infinite plane with a collinear probe position arrangement, the observed voltage offset cannot be attributed to the Hall effect induced by the stray fields of Ni probe [44], since the Hall voltage is perpendicular to the current direction. Furthermore, in the four-probe STM system, the sample and the tips are kept at the same temperature with a temperature gradient $\Delta T < 1$ K [45]; thus, the thermovoltage [46] generated by the different Seebeck coefficients of W and Ni is negligibly small. And the measured spin-chemical potential changes sign when the magnetization direction of Ni probe is reversed [Fig. 3(b)], which also rules out a thermovoltage contribution.

The above discussions are based on an assumption that the electron transport through TSS is in the diffusive limit. When considering effects of ballistic transport on the 2D and 3D components of the conductivity, we obtain a

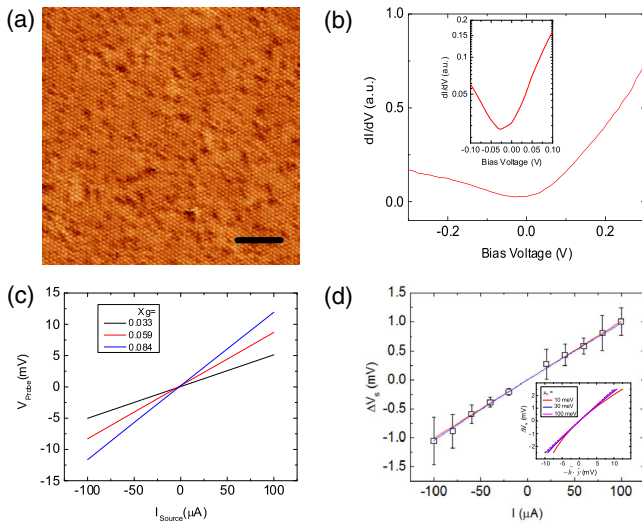


FIG. 4. (a) Topographic STM image of the (001) surface of fresh $\text{Bi}_2\text{Te}_2\text{Se}$ surface (scale bar: 5 nm). (b) Differential conductance (dI/dV) spectra taken on fresh sample showing a minima at -28 meV (Set point: -500 mV, 60 pA). (c) Typical IV curves showing a linear behavior from which the values of R are extracted. (d) ΔV_s vs I plot with a linear fit of data points (red line) and ΔV_s values calculated with Eq. (1) (blue line). Inset shows $-\hbar \cdot \hat{\mathbf{y}}$ vs ΔV_s calculated for different values of Fermi energy (μ_F) using the Eq. (1) with $P_{\text{FM}} = 1$.

ballistic correction (δV_b) to the voltage drop between the two voltage probes as [30]

$$\delta V_b = 2A \sin\left(\frac{\pi s_{23}}{2s_{14}}\right) \sin\left(\frac{\pi(s_{12} - s_{34})}{2s_{14}}\right). \quad (6)$$

During our measurements the inner probes moved towards each other symmetrically by keeping $s_{12} \approx s_{34}$. Therefore, the correction for ballistic transport does not affect the measured ratio of 2D and 3D conductivities. Moreover, the linear expression for ΔV_s is valid both in ballistic and diffusive limits as discussed by Hong *et al.* [39]. Therefore, the results presented above constitute a direct measurement on the spin polarization of the currents carried by the TSS regardless of the nature of the transport.

In summary, we have demonstrated pure 2D spin-dependent conductance on the surface of $\text{Bi}_2\text{Te}_2\text{Se}$ single crystals. By employing spin-polarized four-probe STM transport measurements, we have been able to electrically detect the spin-chemical potential induced by the spin-polarized currents carried by surface states. Spin sensitive four-probe spectroscopy does not only provide an alternative transport method to detect spin momentum locking in TIs but also a unique way to study spin-dependent transport in other surface-supported low- D materials and topological phases.

This research was conducted at the Center for Nanophase Materials Sciences, which is a DOE Office of Science User Facility. The crystal growth and characterization at Purdue was supported by DARPA MESO program (Grant No. N66001-11-1-4107).

* apli@ornl.gov

- [1] L. Fu, C. L. Kane, and E. J. Mele, Topological Insulators in Three Dimensions, *Phys. Rev. Lett.* **98**, 106803 (2007).
- [2] J. E. Moore, The birth of topological insulators, *Nature (London)* **464**, 194 (2010).
- [3] M. Z. Hasan and C. L. Kane, Colloquium: topological insulators, *Rev. Mod. Phys.* **82**, 3045 (2010).
- [4] D. Pesin and A. H. MacDonald, Spintronics and pseudo-spintronics in graphene and topological insulators, *Nat. Mater.* **11**, 409 (2012).
- [5] X.-L. Qi and S.-C. Zhang, Topological insulators and superconductors, *Rev. Mod. Phys.* **83**, 1057 (2011).
- [6] A. Soumyanarayanan, N. Reyren, A. Fert, and C. Panagopoulos, Emergent phenomena induced by spin-orbit coupling at surfaces and interfaces, *Nature (London)* **539**, 509 (2016).
- [7] K. Kondou, R. Yoshimi, A. Tsukazaki, Y. Fukuma, J. Matsuno, K. S. Takahashi, M. Kawasaki, Y. Tokura, and Y. Otani, Fermi-level-dependent charge-to-spin current conversion by Dirac surface states of topological insulators, *Nat. Phys.* **12**, 1027 (2016).
- [8] D. Hsieh, Y. Xia, D. Qian, L. Wray, J. H. Dil, F. Meier, J. Osterwalder, L. Patthey, J. G. Checkelsky, N. P. Ong, A. V. Fedorov, H. Lin, A. Bansil, D. Grauer, Y. S. Hor, R. J. Cava, and M. Z. Hasan, A tunable topological insulator in the spin helical Dirac transport regime, *Nature (London)* **460**, 1101 (2009).
- [9] K. Miyamoto, A. Kimura, T. Okuda, H. Miyahara, K. Kuroda, H. Namatame, M. Taniguchi, S. Eremeev, T. Menshchikova, and E. V. Chulkov, Topological surface states with persistent high spin polarization across the Dirac point in $\text{Bi}_2\text{Te}_2\text{Se}$ and $\text{Bi}_2\text{Se}_2\text{Te}$, *Phys. Rev. Lett.* **109**, 166802 (2012).
- [10] Z. H. Pan, E. Vescovo, A. V. Fedorov, D. Gardner, Y. S. Lee, S. Chu, G. D. Gu, and T. Valla, Electronic Structure of the Topological Insulator Bi_2Se_3 Using Angle-Resolved Photoemission Spectroscopy: Evidence for a Nearly Full Surface Spin Polarization, *Phys. Rev. Lett.* **106**, 257004 (2011).
- [11] J. W. McIver, D. Hsieh, H. Steinberg, P. Jarillo Herrero, and N. Gedik, Control over topological insulator photocurrents with light polarization, *Nat. Nanotechnol.* **7**, 96 (2012).
- [12] C. H. Li, O. M. J. van't Erve, J. T. Robinson, Y. Liu, L. Li, and B. T. Jonker, Electrical detection of charge-current-induced spin polarization due to spin-momentum locking in Bi_2Se_3 , *Nat. Nanotechnol.* **9**, 218 (2014).
- [13] J. Tian, I. Miotkowski, S. Hong, and Y. P. Chen, Electrical injection and detection of spin-polarized currents in topological insulator $\text{Bi}_2\text{Te}_2\text{Se}$, *Sci. Rep.* **5**, 14293 (2015).
- [14] A. Dankert, J. Geurs, M. V. Kamalakar, S. Charpentier, and S. P. Dash, Room temperature electrical detection of spin polarized currents in topological insulators, *Nano Lett.* **15**, 7976 (2015).
- [15] Y. Ando, T. Hamasaki, T. Kurokawa, K. Ichiba, F. Yang, M. Novak, S. Sasaki, K. Segawa, Y. Ando, and M. Shiraishi, Electrical detection of the spin polarization due to charge flow in the surface state of the topological insulator $\text{Bi}_{1.5}\text{Sb}_{0.5}\text{Te}_{1.7}\text{Se}_{1.3}$, *Nano Lett.* **14**, 6226 (2014).
- [16] J. Tang, L.-T. Chang, X. Kou, K. Murata, E. S. Choi, M. Lang, Y. Fan, Y. Jiang, M. Montazeri, and W. Jiang, Electrical detection of spin-polarized surface states conduction in $(\text{Bi}_{0.53}\text{Sb}_{0.47})_2\text{Te}_3$ topological insulator, *Nano Lett.* **14**, 5423 (2014).
- [17] J. S. Lee, A. Richardella, D. R. Hickey, K. A. Mkhoyan, and N. Samarth, Mapping the chemical potential dependence of current-induced spin polarization in a topological insulator, *Phys. Rev. B* **92**, 155312 (2015).
- [18] B. Zhou, Z. Liu, J. Analytis, K. Igarashi, S. Mo, D. Lu, R. Moore, I. Fisher, T. Sasagawa, and Z. Shen, Controlling the carriers of topological insulators by bulk and surface doping, *Semicond. Sci. Technol.* **27**, 124002 (2012).
- [19] M. Koleini, T. Frauenheim, and B. Yan, Gas Doping on the Topological Insulator Bi_2Se_3 Surface, *Phys. Rev. Lett.* **110**, 016403 (2013).
- [20] C. Chen, S. He, H. Weng, W. Zhang, L. Zhao, H. Liu, X. Jia, D. Mou, S. Liu, J. He, Y. Peng, Y. Feng, Z. Xie, G. Liu, X. Dong, J. Zhang, X. Wang, Q. Peng, Z. Wang, S. Zhang, F. Yang, C. Chen, Z. Xu, X. Dai, Z. Fang, and X. J. Zhou, Robustness of topological order and formation of quantum well states in topological insulators exposed to ambient environment, *Proc. Natl. Acad. Sci. U.S.A.* **109**, 3694 (2012).
- [21] P. Li and I. Appelbaum, Interpreting current-induced spin polarization in topological insulator surface states, *Phys. Rev. B* **93**, 220404 (2016).

- [22] E. K. de Vries, A. M. Kamerbeek, N. Koirala, M. Brahlek, M. Salehi, S. Oh, B. J. van Wees, and T. Banerjee, Towards the understanding of the origin of charge-current-induced spin voltage signals in the topological insulator Bi_2Se_3 , *Phys. Rev. B* **92**, 201102 (2015).
- [23] T.-H. Kim, Z. Wang, J. F. Wendelken, H. H. Weitering, W. Li, and A.-P. Li, A cryogenic Quadrupole scanning tunneling microscope system with fabrication capability for nanotransport research, *Rev. Sci. Instrum.* **78**, 123701 (2007).
- [24] A.-P. Li, K. W. Clark, X. G. Zhang, and A. P. Baddorf, Electron transport at the nanometer-scale spatially revealed by four-probe scanning tunneling microscopy, *Adv. Funct. Mater.* **23**, 2509 (2013).
- [25] R. Wiesendanger, Spin mapping at the nanoscale and atomic scale, *Rev. Mod. Phys.* **81**, 1495 (2009).
- [26] M. Bode, Spin-polarized scanning tunnelling microscopy, *Rep. Prog. Phys.* **66**, 523 (2003).
- [27] S. Hasegawa, I. Shiraki, F. Tanabe, and R. Hobarra, Transport at surface nanostructures measured by four-tip STM, *Curr. Appl. Phys.* **2**, 465 (2002).
- [28] H. Cao, C. Liu, J. Tian, Y. Xu, I. Miotkowski, M. Z. Hasan, and Y. P. Chen, Controlling and distinguishing electronic transport of topological and trivial surface states in a topological insulator, [arXiv:1409.3217](https://arxiv.org/abs/1409.3217).
- [29] C. Durand, X. G. Zhang, S. M. Hus, C. Ma, M. A. McGuire, Y. Xu, H. Cao, I. Miotkowski, Y. P. Chen, and A.-P. Li, Differentiation of surface and bulk conductivities in topological insulators via four-probe spectroscopy, *Nano Lett.* **16**, 2213 (2016).
- [30] See Supplemental Material at <http://link.aps.org/supplemental/10.1103/PhysRevLett.119.137202> for derivation of Eq. (1) and Eq. (6), which includes Refs. [31–33].
- [31] R. G. Chambers, The conductivity of thin wires in a magnetic field, *Proc. R. Soc. A* **202**, 378 (1950).
- [32] A. B. Pippard, *The Dynamics of Conduction Electrons* (Gordon and Breach, New York, New York, 1965), p. 57.
- [33] X. G. Zhang and W. H. Butler, Conductivity of metallic films and multilayers, *Phys. Rev. B* **51**, 10085 (1995).
- [34] T. Valet and A. Fert, Theory of the perpendicular magnetoresistance in magnetic multilayers, *Phys. Rev. B* **48**, 7099 (1993).
- [35] P. M. Haney, H.-W. Lee, K.-J. Lee, A. Manchon, and M. D. Stiles, Current induced torques and interfacial spin-orbit coupling: Semiclassical modeling, *Phys. Rev. B* **87**, 174411 (2013).
- [36] M. Y. Veillette, C. Bena, and L. Balents, Spin precession and oscillations in mesoscopic systems, *Phys. Rev. B* **69**, 075319 (2004).
- [37] L. Balents and R. Egger, Spin Transport in Interacting Quantum Wires and Carbon Nanotubes, *Phys. Rev. Lett.* **85**, 3464 (2000).
- [38] B. T. Jonker, A. T. Hanbicki, D. T. Pierce, and M. D. Stiles, Spin nomenclature for semiconductors and magnetic metals, *J. Magn. Magn. Mater.* **277**, 24 (2004).
- [39] S. Hong, V. Diep, S. Datta, and Y. P. Chen, Modeling potentiometric measurements in topological insulators including parallel channels, *Phys. Rev. B* **86**, 085131 (2012).
- [40] Z. Ren, A. Taskin, S. Sasaki, K. Segawa, and Y. Ando, Large bulk resistivity and surface quantum oscillations in the topological insulator $\text{Bi}_2\text{Te}_2\text{Se}$, *Phys. Rev. B* **82**, 241306 (2010).
- [41] S. Just, H. Soltner, S. Korte, V. Cherepanov, and B. Voigtländer, Surface Conductivity of Si(100) and Ge(100) Surfaces Determined from Four-Point Transport Measurements Using an Analytical N-Layer Conductance Model, [arXiv:1610.02239](https://arxiv.org/abs/1610.02239).
- [42] J. Park, C. Park, M. Yoon, and A.-P. Li, Surface magnetism of cobalt nanoislands controlled by atomic hydrogen, *Nano Lett.* **17**, 292 (2017).
- [43] S. F. Alvarado, Tunneling Potential Barrier Dependence of Electron Spin Polarization, *Phys. Rev. Lett.* **75**, 513 (1995).
- [44] D. H. Petersen, O. Hansen, R. Lin, and P. F. Nielsen, Micro-four-point probe Hall effect measurement method, *J. Appl. Phys.* **104**, 013710 (2008).
- [45] K. W. Clark, X.-G. Zhang, G. Gu, J. Park, G. He, R. M. Feenstra, and A.-P. Li, Energy Gap Induced by Friedel Oscillations Manifested as Transport Asymmetry at Monolayer-Bilayer Graphene Boundaries, *Phys. Rev. X* **4**, 011021 (2014).
- [46] J. Park, G. He, R. M. Feenstra, and A.-P. Li, Atomic-scale mapping of thermoelectric power on graphene: role of defects and boundaries, *Nano Lett.* **13**, 3269 (2013).